RADIOLOGICAL CHARACTERIZATION OF ALKALI-ACTIVATED MATERIAL DOPED WITH Sm_2O_3 AND ITS POLYMERIZATION PRODUCTS

by

***Sanja V. KNEŽEVIĆ*[1], *Marija M. IVANOVIĆ*[1], *Snežana S. NENADOVIĆ*[1], *Milica M. RAJAČIĆ*[2], *Marijan NEČEMER*[3], *Jelena POTOČNIK*[4], *and Miloš T. NENADOVIĆ*[4*]**

[1] Department of Materials, Vinča Institute of Nuclear Sciences,
National Institute of the Republic of Serbia, University of Belgrade, Vinča, Belgrade, Serbia
[2] Department of Radiation and Environmental Protection, Vinča Institute of Nuclear Sciences,
National Institute of the Republic of Serbia, Vinča, Belgrade, Serbia
[3] Department of Low and Medium Energy Physics, Jožef Stefan Institute, Ljubljana, Slovenia
[4] Department of Atomic Physics, Vinča Institute of Nuclear Sciences,
National Institute of the Republic of Serbia, University of Belgrade, Vinča, Belgrade, Serbia

Scientific paper
https://doi.org/10.2298/NTRP2404280K

The aim of this study was determination of radiological characterization of alkali-activated material with Sm_2O_3 and its polymerization products. Alkali-activated materials with 1 wt.% and 5 wt.% addition of Sm_2O_3 were synthesized and their natural radioactivity was determined. Energy dispersive X-ray fluorescence showed changes in the phase composition, or the formation of stable compounds, at higher temperatures. All samples demonstrated good pozzolanic activity, while the percentage of Sm_2O_3 was slightly changed. The X-ray photoelectron spectroscopy confirmed that the obtained material has a very low carbon content making it environmentally friendly, due to its low carbon content. A detailed analysis of the oxygen peak indicates variations in the stoichiometry of the oxides, which may affect the changes of natural radioactivity. Scanning electron microscopy confirmed that with the increase in the temperature of the thermal treatment, the opening of the pores in the alkali-activated material occurs, as well as further propagation of reaction that increased porosity and crystallization. Radiological measurement confirmed that examined alkali-activated material is safe for usage and exploitation. It should be emphasized that the presence of artificial radionuclide cesium ^{137}Cs was not detected.

Key words: alkali-activated material, Sm_2O_3, gamma-ray spectrometry, energy dispersive X-ray fluorescence, X-ray photoelectron spectroscopy

INTRODUCTION

In the last few years, alkali-activated materials (AAM) have become an increasingly important research subject due to their exceptional mechanical properties, excellent corrosion resistance, and high durability, which is especially important for high-temperature applications [1]. The AAM are known as alkali-aluminosilicate cementitious materials that can exhibit superior mechanical, chemical, and thermal properties compared to Portland cement-based cements, with significantly lower CO_2 emissions during production [2]. According to the available literature, AAM demonstrate greater durability than Portland cement at temperatures between 600 °C and 800 °C and even at higher temperatures [3]. After alkali-activation, AAM form a cage-like closed cavity structure, which, together with a combination of ring molecules, can encapsulate metal ions or other toxic substances and trap them inside the cavity [4, 5]. Despite this, some metal cations can participate in the polymerization reaction. Previous studies have shown promising results in the treatment of toxic metals by immobilizing into an alkali-activated structure [6-9]. Ivanović *et al*. [10] examined the thermodynamic parameters (viscosity, density, refractive index, speed of sound) of the alkali activator and examined the influence on the synthesis of geopolymers. It was confirmed that, with the knowledge of the thermodynamic parameters, there is a better understanding of the first stage of gel formation of the AAM structure. In previous research by Nenadović *et al*. [11] and Kljajević *et al.* [12], the synthesis and struc-

* Corresponding author, e-mail: milosn@vin.bg.ac.rs

ture of AAM, the influence of AAM were examined focusing on the influence of changes in the aluminosilicate matrix and the alkaline activator [13]. Materials with 12 M NaOH have been the most common subjects. The aim of this work is to examine the effect of Sm in the form of its oxide, and incorporation during the initial phase of gelation of the geopolymer structure. Interest in developing AAM is motivated by economic advantages as the process allows the use of industrial by-products (slag, fly-ash) and natural clays, and kaolin, to produce a material with significant added value that is competitive with Portland cement [14]. Building materials play various roles in construction, so they should have appropriate properties. Mineralogical and chemical composition of the raw materials influences fundamental properties (physico-chemical, mechanical, and long-lasting) of building materials [15]. Since these materials are usually considered as naturally occurring radioactive materials (NORM), the radiological aspect of their use as building materials should also be taken into account [16]. Determining the content of natural radionuclides in building materials is important for assessing the radiation exposure of people, who can spend up to 80 % of their time indoors [17, 18]. Terrestrial radiation in buildings originates not only from the soil [19, 20] but also from the building materials used [21, 22]. For the last few decades, radiological research related to construction materials and buildings and their impact on human health has been supported. Building materials strongly influence indoor levels of the radioactive gas radon – a direct descendant of ^{226}Ra, and its decay products, which contribute significantly to total inhalation doses. International studies by the World Health Organization (WHO) [23] and the International Commission on Radiological Protection [24] show that building materials have a non-negligible share in the public's exposure to radiation due to radon. Depending on the material, the concentration of natural radionuclides (mainly ^{226}Ra, ^{232}Th, and ^{40}K) ranges from 1 Bqkg^{-1} to 4000 Bqkg^{-1} [25]. In the focus of the research of Ivanović *et al*. [16] was kaolin, which was the subject of their previously published work [26], and its polymerization products – AAM. The structural characteristics of precursor materials and AAM samples were investigated using different analytical techniques. The DRIFT and XPS analyses were used to monitor the formation of new chemical bonds during the synthesis of geopolymers as potential construction material. Gamma spectroscopic measurements of a set of samples (kaolin, metakaolin and geopolymer) determined the activity of natural radionuclides (^{226}Ra, ^{232}Th, and ^{40}K). One of the challenges is the fact that, despite the large number of studies and increasing attention on AAM, they are not fully elucidated, since the polymerization process of AAM and the structure itself are not yet fully understood, considering the variety of precursors that can serve as the basis for obtaining these type of material. This work focuses on paying more attention to the structural, chemical, and radiological characteristics of the obtained AAM samples.

EXPERIMENTAL

Materials and methods

The used kaolin is high clay obtained from Serbia. The physicochemical and radiological characterization of kaolin and its polymerization products were investigated in previous work by Nenadović *et al*. [18] and Ivanović *et al.* [16]. It was shown that the structural characteristics of this kaolin are suitable for mechanochemical, radioactivity, and thermal treatment planned in this research. The alkaline solution was prepared from sodium silicate (volume ration Na_2SiO_3/NaOH = 1.6) and 12 M NaOH. The reference alkali activated was formed from metakaolin, 1 wt.% or 5 wt.% Sm_2O_3, and the alkaline solution (solid/liquid ratio was 0.85), mixed for 10 minutes and then left at room temperature for one day. Finally, the mixture was kept in a sample drying oven for two days at constant temperature 50 °C. A time of 28 days is necessary to complete the process of polymerization.

In this research, 8 samples (S1-S8) were synthesized. Sample S1 was synthesized with 1 wt.% Sm_2O_3, while sample S2 was synthesized with 5 wt.% Sm_2O_3. Samples from S3 to S8 were thermally treated at temperatures of 300 °C, 600 °C, and 900 °C. The synthesis results are presented in tab. 1.

CHARACTERIZATION TECHNIQUES

Energy dispersive X-ray fluorescence spectrometry

Energy dispersive X-ray fluorescence (EDXRF) is a rapid, straightforward, and cost-effective non-destructive technique for multielement analysis. For this process, the pulverized sample was pressed into a pellet and analyzed directly using an XRF spectrometer equipped with three monochromatic excitation sources built in-house: ^{55}Fe, ^{109}Cd, and ^{241}Am. This configuration of monochromatic excitation sources allows for optimal excitation across a range of elements, from light

Table 1. The chart of synthesized samples

Number	Code of the sample	Amount of Sm_2O_3 [wt.%]	Thermal treatment temperature [°C]
1	S1	1 Sm_2O_3	–
2	S2	5 Sm_2O_3	–
3	S3	1 Sm_2O_3	300
4	S4	5 Sm_2O_3	300
5	S5	1 Sm_2O_3	600
6	S6	5 Sm_2O_3	600
7	S7	1 Sm_2O_3	900
8	S8	5 Sm_2O_3	900

elements such as sodium (Na) and potassium (K) to heavier elements such as samarium (Sm). The resulting fluorescence radiation was detected using EDXRF spectrometers with SDD or Si(Li) detectors. Details on the spectrometer configuration and the quantitative analysis software used are available in the referenced sources [27, 28].

Diffuse reflectance infrared Fourier transform spectroscopy

The DRIFT spectra were obtained using a Perkin-Elmer FTIR spectrometer. Approximately 5 % of the samples were dispersed in dry, spectroscopic KBr with a refractive index of 1.559 and a particle size of 5-20 μm. Baseline KBr spectra were obtained, and spectra were rationed to the background. The spectra were scanned at a resolution of 4 cm^{-1} and collected in the mid-IR region from 4000 cm^{-1} to 400 cm^{-1}.

The X-ray photoelectron spectroscopy

The X-ray photoelectron spectroscopy (XPS) was performed using a SPECS instrument for X-ray photoelectron spectroscopy by monochromatic Al Kα line with a photon energy of 1486.67 eV. Detailed spectra of the main photoelectron lines were taken in the fixed analyzer transmission mode with a pass energy of 20 eV (FAT 20), an energy step of 0.1 eV, and a dwell time of 2 seconds. Charging compensation was performed using an electron flood gun and the constant current and voltage. The survey spectra were performed according to the characteristic spectral line intensities.

Scanning electron microscopy

An emission scanning electron microscope (FESEM, FEIScios 2, DualBeamsystem) was used for morphological examinations. The samples were attached to the sample holder using double-sided copper tape. Micrographs were taken at an accelerating voltage of 15 kV and a chamber pressure of approximately $9 \cdot 10^{-5}$ Pa.

Gamma-ray spectrometry

The radiological characterization of the synthesized samples was performed using the gamma spectrometric method. This method is used to identify gamma emitter radionuclides present in the tested samples, as well as determination their specific activity. Measurements were carried out in accordance with international recommendations [29]. The measurements were performed on a semiconductor HPGe spectrometer (Canberra, relative efficiency 18 % and resolution 1.8 keV at 1332 keV) and, due to the achievement of the appropriate measurement uncertainty, lasted 60000 s each. The preparation of reference radioactive material for spectrometer efficiency calibration according to the recommendations of the International Atomic Energy Agency (IAEA) [30] was carried out using a certified solution of a mixture of gamma emitting radionuclides (^{241}Am, ^{109}Cd, ^{139}Ce, ^{57}Co, ^{60}Co, ^{137}Cs, ^{133}Ba, ^{85}Sr, ^{51}Cr, ^{210}Pb, and ^{88}Y) produced by the Czech Meteorology Institute (CMI). The spectra of the tested samples were recorded using the Genie2000 software package (Canberra). Energy calibration was performed with reference point standards ^{133}Ba and ^{60}Co.

RESULTS AND DISCUSSION

Energy dispersive X-ray fluorescence spectrometry

Quantitative EDXRF chemical analysis determined the percentage composition of oxides in samples S1-S8. The results in tab. 2. show a high level of silicon(IV)-oxide (SiO_2), aluminum(III)-oxide (Al_2O_3), sodium oxide (Na_2O), and iron(III)-oxide (Fe_2O_3). Based on the literature [31], good pozzolanic activity of

Table 2. Chemical composition of AAM

Oxides	Samples							
	Non-treated		Thermally treated [°C]					
			Sm_2O_3 1wt.%			Sm_2O_3 5wt.%		
	Sm_2O_3 1wt.%	Sm_2O_3 5wt.%	300	600	900	300	600	900
	S1	S2	S3	S5	S7	S4	S6	S8
Na_2O [%]	16.95	14.33	15.53	18.09	15.02	18.50	18.23	16.36
MgO [%]	1.81	3.16	2.80	0.99	1.86	2.04	1.67	2.17
Al_2O_3 [%]	23.76	24.19	23.72	22.83	24.39	23.28	22.46	22.57
SiO_2 [%]	53.11	51.89	53.50	53.54	53.67	52.50	51.25	51.72
K_2O [%]	1.55	1.53	1.53	1.65	1.72	1.50	1.49	1.63
CaO [%]	0.29	0.29	0.29	0.29	0.35	0.28	0.28	0.30
TiO_2 [%]	0.26	0.21	0.47	0.46	0.53	0.42	0.43	0.45
Fe_2O_3 [%]	1.53	1.41	1.46	1.47	1.68	1.41	1.40	1.56
Sm_2O_3 [%]	0.63	2.89	0.61	0.59	0.68	2.85	2.70	3.13

the material requires that the content of silicon, aluminum, and iron oxides (SiO_2+ Al_2O_3+ Fe_2O_3) be greater than 70 % and that the material contains as much of the amorphous phase as possible. All the samples have good pozzolanic activity because the sum of silicon, aluminum, and iron oxides (SiO_2+ Al_2O_3 + Fe_2O_3) is greater than 70 %. Pozzolanic activity for untreated samples is S1 = 78.40 % and S2 = 77.49 %.

Table 2 shows the percentages of oxides present in thermally treated samples in which Sm_2O_3 was incorporated. As with samples that were not thermally treated, it is observed that the largest contribution is made by silicon, aluminum, and sodium oxide, which are characteristic of aluminosilicate materials. Elevated temperatures generally increase the percentage of oxides such as Na_2O, Al_2O_3, SiO_2, and TiO_2. These changes indicate changes in the phase composition, or the formation of stable compounds, at higher temperatures. All the samples show a good pozzolanic activity, meeting the standard of the American Society for Testing of Cementitious Materials (ASTM C618) [32] with a combined content of SiO_2, Al_2O_3, and Fe_2O_3 exceeding 70 %. The thermally treated samples show slightly different results, which indicates that the thermal treatment affects the pozzolanic activity of the material. The results of the pozzolanic activity for the thermally treated samples are for S3 = 78.68 %, S4 = 77.19 %, S5 = 77.84 %, S6 = 75.11 %, S7 = 79.74 %, S8 = 75.85 %. Based on the results, it can be concluded that pozzolanic activity increases in samples with 1 wt.% Sm_2O_3, while pozzolanic activity decreases in samples with 5 wt.% Sm_2O_3.

The thermal treatment causes slight changes compared to the basic samples, such as the percentage composition Sm_2O_3, which in some samples show an increase, while the MgO content decreases, which indicates possible phase changes. Oxides such as Al_2O_3, SiO_2, K_2O, and CaO remain stable, indicating thermal stability.

Diffuse reflectance infrared Fourier transform spectroscopy

The graph in fig. 1 shows the DRIFT reflectance spectra of geopolymer samples with incorporated 1 wt.% Sm_2O_3, the samples were analyzed at different temperatures: S1 (non-thermally treated), S3 (300 °C), S5 (600 °C), and S7 (900 °C). The adsorption of CO_2 from the atmosphere is also observed in fig. 1, the vibrational bands attributed to this are located at 2793 cm^{-1} and 1470 cm^{-1} [33, 34]. The assignation of the band at 1030 cm^{-1} is characteristic of Si-O-T (T = Si or Al) asymmetric vibrations. The stretching vibration of Sm-O occurs at 796 cm^{-1}. The confirmation of the Sm-OH bond formation is the assignment of the Sm-OH bending vibration band at 669 cm^{-1}. The stretching vibration of Sm-O-Si is visible in the 561 cm^{-1} vibrational band [35]. The S1 remains in its original, less modified form, with the highest reflectance. Samples S3, S5, and S7 show structural changes, with reorganization of the silicate network as the temperature rises. The trend is clear: higher temperatures lead to more significant structural modifications, with S7 showing the most changes, likely due to crystallization or partial sintering at 900°.

The graph in fig. 2 shows the DRIFT reflectance spectra of geopolymer samples with incorporated 5 wt.% Sm_2O_3, the samples were analyzed at different temperatures: S2 (non-thermally treated), S4 (300 °C), S6 (600 °C), and S8 (900 °C). The values of the wavenumbers remained almost the same; there is a difference in the band characteristic for forming the Sm-OH bond; its value after thermal treatment is 3623 cm^{-1}. Also, the bands for carbon- dioxide adsorption from the atmosphere have 2784 cm^{-1} and 1475 cm^{-1} wavenumber values.

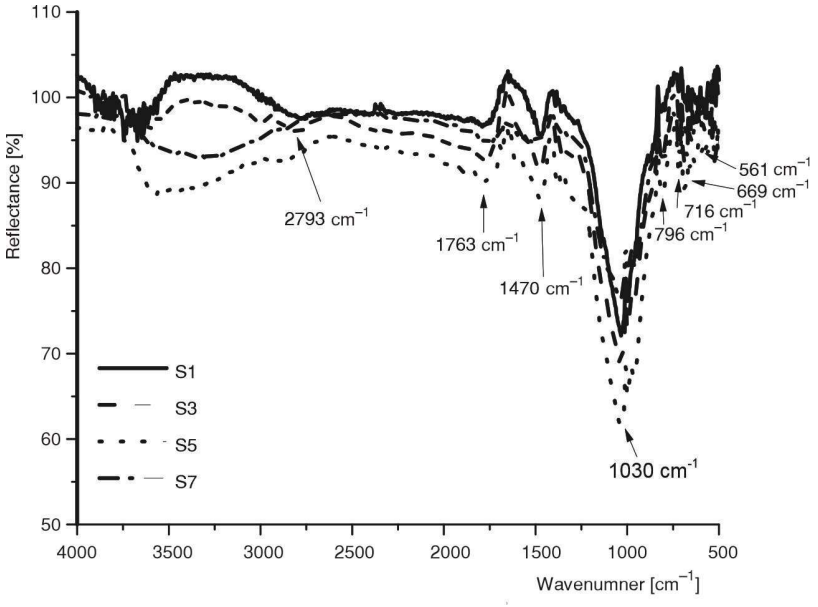

Figure 1. The DRIFT reflectance spectra of geopolymer samples with incorporated 5 wt.% Sm_2O_3, the samples were analyzed at different temperatures; S1 (non-thermally treated), S3 (300 °C), S5 (600 °C), and S7 (900 °C)

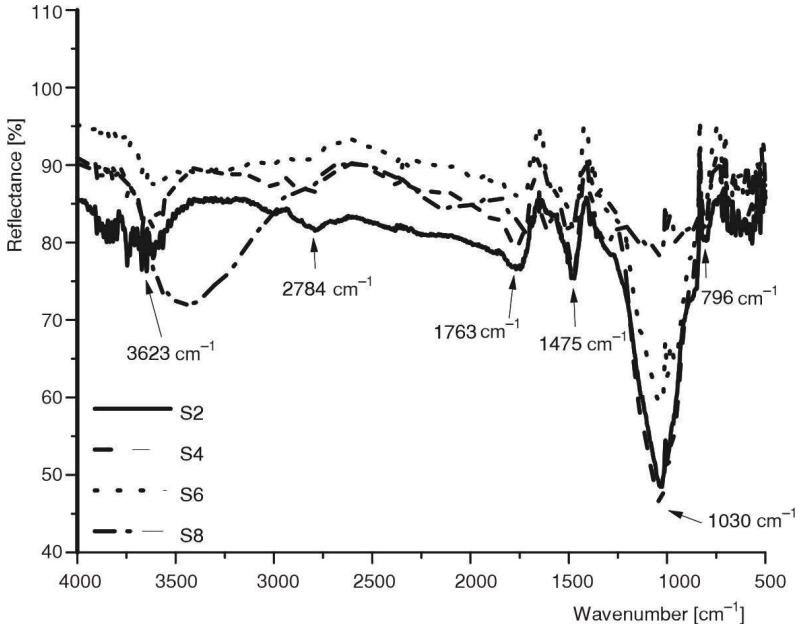

Figure 2. The DRIFT reflectance spectra of geopolymer samples with in corporated 5 wt.% Sm_2O_3, the samples were analyzed at different temperatures; S2 (non-thermally treated), S4 (300 °C), S6 (600 °C), and S8 (900 °C)

At wave numbers 1033 cm^{-1}, 807 cm^{-1}, and 669 cm^{-1}, there are vibrations corresponding to Si-O-T, Sm-O, and Sm-O-H bonds, respectively.

The X-ray photoelectron spectroscopy

The XPS analysis of aluminosilicate materials is quite demanding. Due to its insulating properties, non-uniform surface charging occurs, which results in peak broadening. For this reason, one should be very careful when talking about this type of characterization because materials of natural origin are generally multiphase.

Figure 3(a) shows the survey spectrum of AAM treated at 300 °C. The most dominant spectral line belongs to oxygen O 1s, while very pronounced peaks for aluminum Al 2p, and silicon Si 2p are also visible due to the chemical composition of the material. The presence of samarium can also be seen from the survey spectrum at binding energy around 1100 eV. From the same image, it can be seen that the carbon peak practically does not exist. This speaks in favor of the fact that this is effectively a carbon-free material.

Figure 3(b) shows the O 1s spectral line of the AAM treated at 300 °C, which has been resolved into two contributions (O1s-1 and O 1s-2). The first more prominent contribution of O 1s-1 at 531.2 eV belongs to siloxo (Si-O-Si) and sialate bonds (Si-O-Al). Another contribution of O 1s-2 at 529.1 eV can be attributed to Si-OH and Si-ONa bonds. From the graph, it can be concluded that the great majority of chemical bonds in AAM are siloxo and show stability at elevated temperatures, figs. 3(c) and 3(d). The O 1s-1 contribution shows that it represents the basic matrix of AAM and that it does not suffer major chemical changes with conditions. As for the second contribution, O1s-2, it shows an irregular trend with increasing temperature. At 600°C, the O1s-2 contribution drops considerably, fig. 3(c), while at 900 °C, fig. 3(d), it reappears in a higher percentage (about 20 %). This indicates that at the maximum treatment temperature, Si-OH and Si-ONa chemical bonds are regenerated to a higher extent compared to the lowest treatment temperature.

Scanning electron microscopy (SEM)

The SEM micrograph at 1200x magnification, fig. 4(a) shows the overall morphology of sample S1. The particles have irregular shapes with variable sizes. The surface is heterogeneous, which indicates a composite material with a porous structure.

After heat treatment at 300 °C, fig. 4(b), the structure becomes more compact. The surface is still uneven, but the pores are more pronounced, and slight cracks in the structure of the material are noticeable. Heat treatment at 300 °C leads to slight compaction of the particles, which could be attributed to a slight ordering of the crystal structure at high temperatures [36]. Treatment at 600 °C, fig. 4(c), additionally changes the morphology; the particles become larger, and a greater degree of sintering occurs. The surface becomes smoother, which indicates thermal stabilization. The micro-structure shows porosity, and the presence of an initial phase of crystallization within the matrix is possible [36]. By increasing the temperature of the thermal treatment, the effect of pore expansion and crystallization of the sample occurs. Thermal treatment at 900 °C contributed to the visible crystallization of the sample. The structure has become more homogeneous, with a smooth surface and porosity, as shown in fig. 4(d).

The sample doped with 5 wt.% Sm_2O_3, fig. 5(a), shows a similar structure to the sample with 1 wt.%

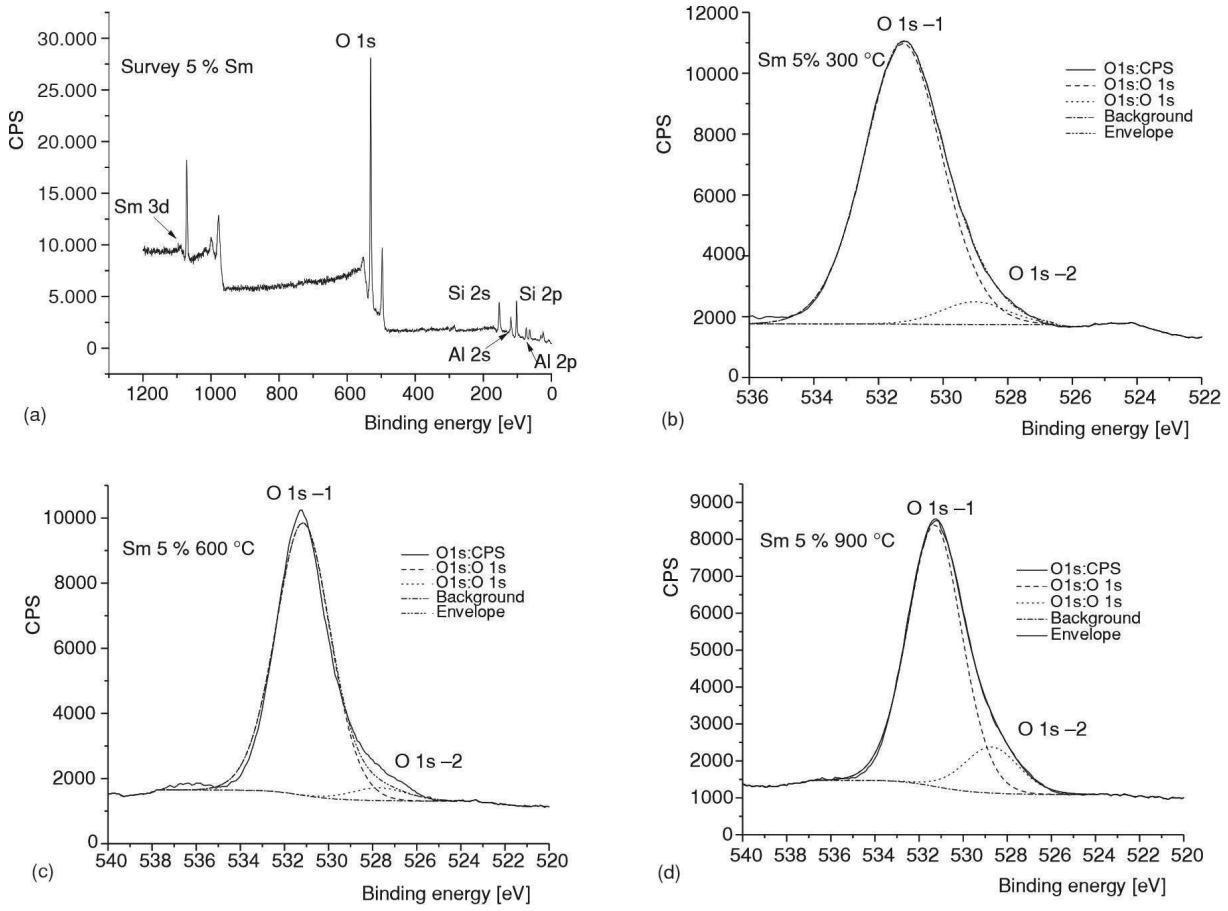

Figure 3. The XPS analysis of AAM with 5 wt.% Sm; (a) Survey XPS spectrum, (b) O 1s 300 °C, (c) O 1s 600 °C, and (d) O 1s 900 °C

Sm_2O_3, but with larger agglomerates. The particles are coarser and have less sharp edges. Porosity is present, but the particles appear more stable and compact. At a temperature of 300 °C, compaction and consolidation of the structure occurs, a similar trend to the sample with 1 wt.% Sm_2O_3, but with the presence of a higher concentration of Sm_2O_3, the structure appears more stable. Porosity is still present, fig. 5(b), with a higher number of open pores compared to the lower dopant sample, fig. 4(b). A similar sintering trend is observed in both samples, but the sample with 5 wt.% Sm_2O_3 in fig. 5(c) shows a clearer crystalline phase and a more homogeneous micro-structure. Also, compared to the sample thermally treated at 600 °C with 1 wt.% Sm_2O_3, the sample with 5 wt.% Sm_2O_3 has a more pronounced tendency to expand the pores. This sample appears more stable at this temperature. At 900 °C, the sample with 5 wt.% Sm_2O_3 in fig. 5(d) shows crystallization [36] and a more stable structure compared to the sample with 1 wt.% Sm_2O_3 in fig. 4(d). There are fewer pores and irregularities, which indicates better thermal stability due to a higher amount of Sm_2O_3. The presence of Sm_2O_3 in geopolymers significantly affects their morphology, especially at higher concentrations and higher temperatures of thermal treatment.

Gamma spectrometric analysis

It is known that all building materials contain different activities of natural radionuclides. Given that the synthesized aluminosilicate materials have a potential application in construction, the specific activity of radionuclides for thermally untreated samples was determined and the results are presented in tab. 3. Measurement uncertainty are given at the 95 % confidence level ($k = 2$).

Given that a natural material, metakaolin, was used for the synthesis of aluminosilicate material, the presence of ^{137}Cs could be expected, which was found in nature partly after the nuclear tests, and to the greatest extent after the accident in Chernobyl. However, tab. 3 shows that the specific activity of this radionuclide was below the detection minimum. Also, no other produced radionuclide was detected.

As the aim of this investigation was to examine whether AAM are safe for use in construction from a radiological aspect, the recommendations of the European Commission on the principles of radiological protection concerning the natural radioactivity of building materials [37] were respected. There it is stated that as a screening method should be used activity concentration index (ACI) determination. An ACI

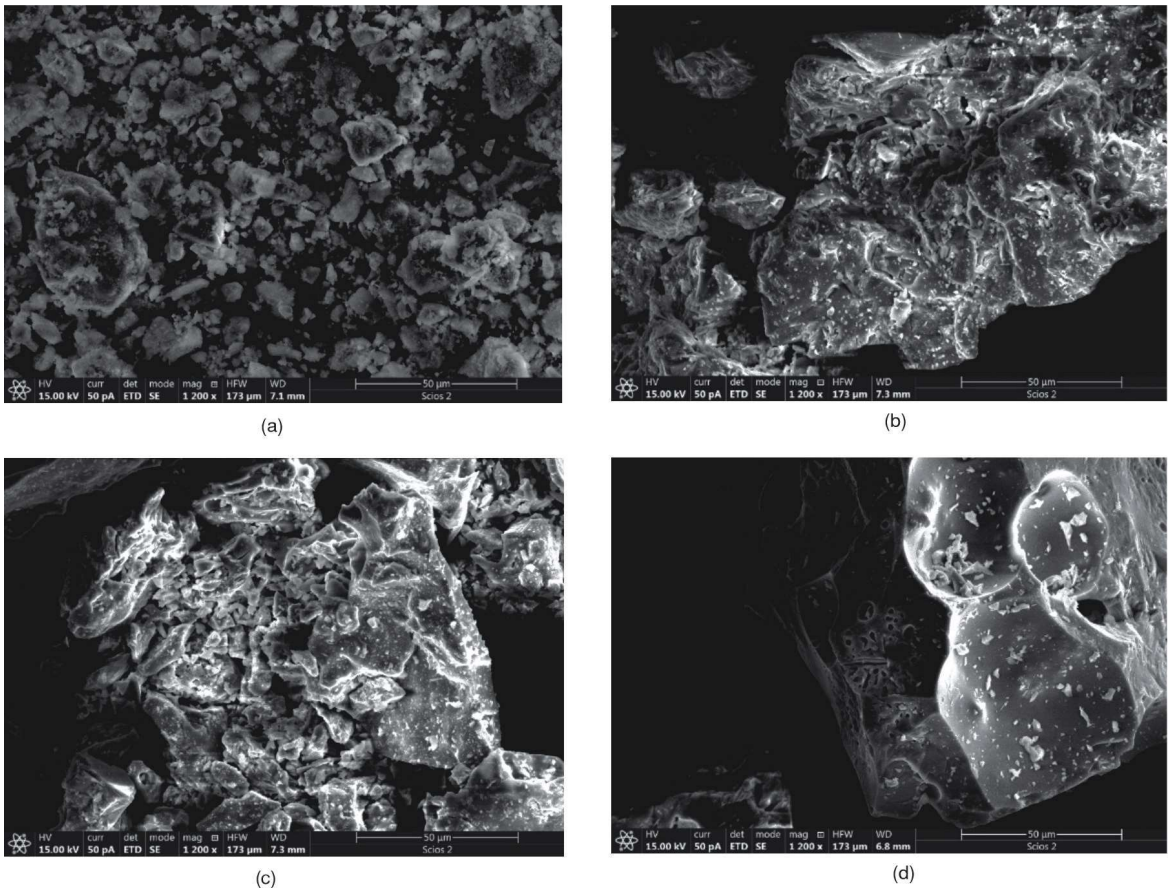

Figure 4. The SEM micrographs at the magnification 1200x; (a) S1, (b) S3, (c) S5, and (d) S7

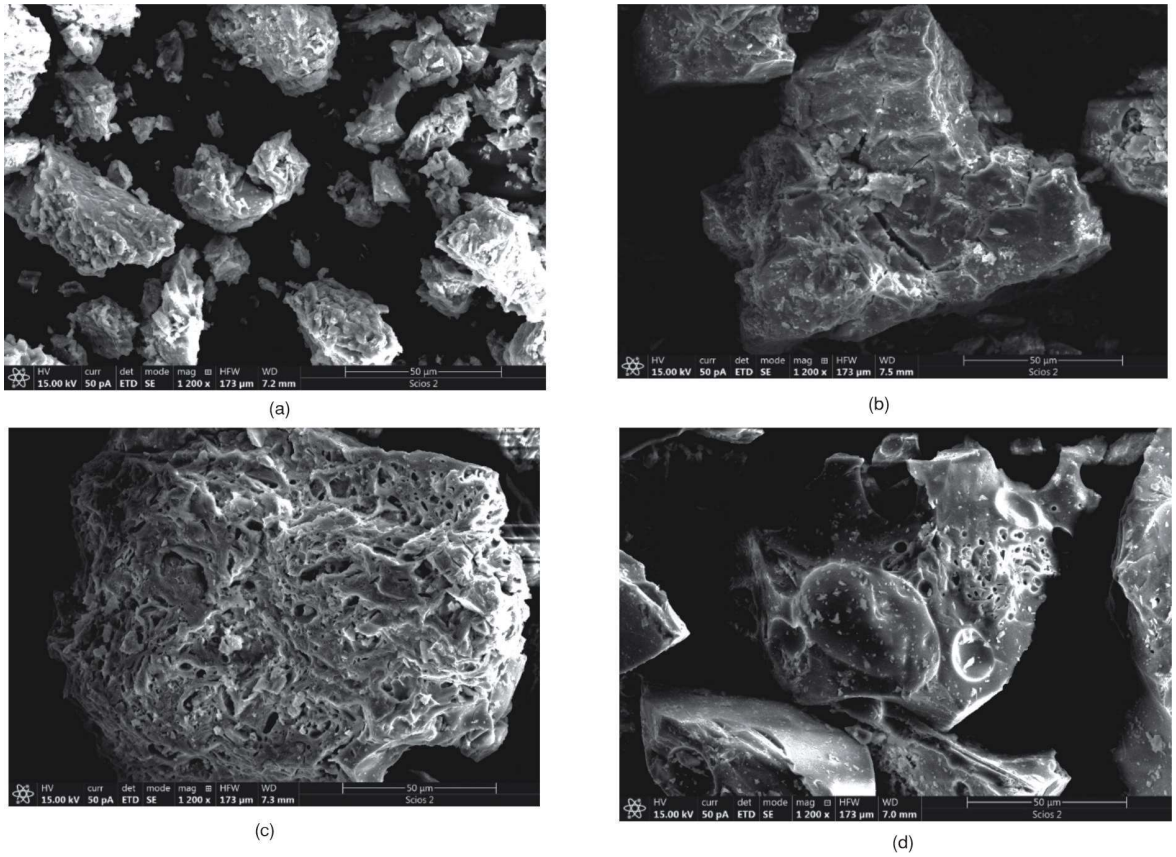

Figure 5. The SEM micrographs at the magnification 1200x; (a) S2, (b) S4, (c) S6, and (d) S8

Table 3. Specific activities of radionuclides in thermally untreated samples with measurement uncertainties (k = 2)

Radionuclide [Bqkg^{-1}]	Thermally untreated samples	
	1 wt.% Sm_2O_3	5 wt.% Sm_2O_3
	S1	S2
^{210}Pb	146 ± 32	240 ± 37
^{226}Ra	96 ± 12	106 ± 13
^{238}U	184 ± 38	<160
^{235}U	16 ± 6	<12
^{228}Ac(^{232}Th)	66 ± 24	<40
^{40}K	443 ± 106	262 ± 83
^{137}Cs	<3	<3

value of less than 1 ensures that the internal annual effective dose rate E, originating from the tested material, if all the structures of the room are made of it, will be less than 1 mSv per year. If the ACI is greater than 1, it is necessary to evaluate the E for other possibilities (or a specific case) of using the tested material. In addition to ACI, Hint was also calculated, which is more rigorous in terms of ^{226}Ra concentration, because it also takes into account the dose received by inhaling radon and its descendants (radon is considered the second cause of lung cancer, after cigarettes).

The E is calculated by eq. (1) [37], using a conversion coefficient of 0.7 SvGy^{-1} to convert the absorbed dose in the air into the effective dose in the human body. The D is the absorbed dose in the air and p·t is annual exposure time, where p is the percentage of years during which humans are exposed to radiation and t is 8.760 hours (number hour in year)

$$E(\text{mSv per year}) = D\left(\frac{\text{nGy}}{\text{h}}\right)\cdot \cdot \text{p}\cdot t(\text{h per year})\cdot 0.7\left(\frac{\text{Sv}}{\text{Gy}}\right)\cdot 10^{-6} \quad (1)$$

For estimate indoor effective dose rate (E_{indoor}, $E_{80\ \%}$) calculation takes into account that the people spend about 80 % of the time indoors (indoor occupancy factor p is 0.8) [37].

The absorbed dose in the air, D (nGyh^{-1}), is estimated based on eq. (2) [37], where are: q_i specific dose rate for isotope i in (nGyh^{-1})/(Bqkg^{-1}) and A_i the activity concentration of isotope i in Bqkg^{-1}

$$D = q_{226_{\text{Ra}}}\cdot A_{226_{\text{Ra}}} + q_{232_{\text{Th}}}\cdot A_{232_{\text{Th}}} + q_{40_{\text{K}}}\cdot A_{40_{\text{K}}} \quad (2)$$

Value of q_i are usually calculated by simulating of different cases. To calculating q_i for estimate absorbed dose of building material, the most frequently used is a standard model room (a room of 20 m^2 and 2.8 m in height). An ACI value less than 1, eq. (3), ensures that E will be less than 1 mSv per year if all the structures of the room (floor, walls and ceiling) are made of tested material

$$ACI = \frac{A_{226_{\text{Ra}}}}{300} + \frac{A_{232_{\text{Th}}}}{200} + \frac{q_{40_{\text{K}}}}{3000} \quad (3)$$

For some cases they are too strictly defined, so these are only screening parameters. When ACI is greater than 1, it is necessary to estimate the dose for the situation in which the observed material is used, for example if they are used for construction only parts of the room: floor and walls (D_{fw}), floor only (D_{f}), surface material for all walls (D_{sup}). Estimates of absorbed dose for these cases where made using eqs. (4)-(6), respectively [37]

$$D_{\text{fw}} = 0.67\cdot A_{226_{\text{Ra}}} + 0.78\cdot A_{232_{\text{Th}}} + 0.057\cdot A_{40_{\text{K}}} \quad (4)$$

$$D_{\text{f}} = 0.24\cdot A_{226_{\text{Ra}}} + 0.28\cdot A_{232_{\text{Th}}} + 0.02\cdot A_{40_{\text{K}}} \quad (5)$$

$$D_{\text{sup}} = 0.12\cdot A_{226_{\text{Ra}}} + 0.14\cdot A_{232_{\text{Th}}} + 0.0096\cdot A_{40_{\text{K}}} \quad (6)$$

In addition to the external radiation, radon and its short-lived products are also hazardous to respiratory organs, and that is quantified by internal hazard index H_{int}, eq. (7), [22]. The value of H_{int} should be less than 1, for material used indoor

$$H_{\text{int}} = \frac{A_{226_{\text{Ra}}}}{185} + \frac{A_{232_{\text{Th}}}}{259} + \frac{q_{40_{\text{K}}}}{4180} \quad (7)$$

Table 4 shows the parameters of radiological safety for samples of synthesized aluminosilicates.

Calculated radiological safety parameters indicate an acceptable radiological risk for use these materials for building, *i.e.* annual effective dose of radiation to the human body originating from the interior of standard room (4 × 5 × 2.8) m with all structures (floor, ceiling and walls) built with them is for both samples below the limit of 1 mSv, each [37, 38].

The specific activities of radionuclides in thermally treated samples were determined by gamma spectrometric analysis and presented in tab. 5. As mentioned, all building materials contain different activities of natural radionuclides. All present radionuclides ^{210}Pb, ^{226}Ra, ^{238}U, ^{235}U show moderate deviations from the usual values according to UNSCEAR [17] and do not represent any alarming data. Also, as in all previous samples, the presence of artificial radionuclide ^{137}Cs was not detected.

The ACI and H_{int} are greater than 1 for samples S5-S8, which indicates that additional assessments of radiological hazard are needed to examine in which cases the materials are suitable for internal use in construction.

As can be seen from tab. 6, all tested heat-treated samples are acceptable from a radiological point of view if they are used for construction the next parts of room: floor and walls, floor only, surface material for

Table 4. Radiological safety parameters of thermally untreated samples: ACI and H_{int}

Radiological safety parameters	Thermally untreated samples	
	1 wt.% Sm_2O_3	5 wt.% Sm_2O_3
	S1	S2
ACI	0.798	0.641
H_{int} [Bqkg^{-1}]	0.865	0.778

Table 5. Specific activities of radionuclides in thermally treated samples with measurement uncertainties (k = 2)

Radionuclide [Bqkg^{-1}]	Thermally treated samples					
	Sm_2O_3 1 wt.%			Sm_2O_3 5 wt.%		
	S3 (300 °C)	S5 (600 °C)	S7 (900 °C)	S4 (300 °C)	S6 (600 °C)	S8 (900 °C)
^{210}Pb	166 ±28	173 ±30	90 ±20	113 ±22	248 ±31	<25
^{226}Ra	86 ±11	200 ±10	150 ±10	81 ±10	135 ±29	133 ±9
^{238}U	277 ±37	190 ±30	124 ±28	200 ±30	140 ±30	108 ±23
^{235}U	15 ±3	17 ±2	12.8 ±1.8	11 ±2	8 ±1	7.7 ±1.1
^{228}Ac(^{232}Th)	<30	85 ±16	73 ±14	65 ±20	90 ±20	80 ±14
^{40}K	320 ±80	720 ±90	625 ±75	<190	642 ±84	629 ±75
^{137}Cs	<3	<2	<1	<3	<2	<1

Table 6. Radiological safety parameters: the ACI and H_{int}, absorbed dose in the air (D) and annual effective dose from inside (E_{indoor}) for three different cases of possible use of thermally treated samples (floor and walls, only floor, superficial material for all walls)

Radiological safety parameters	Thermally treated samples					
	Sm_2O_3 1 wt.%			Sm_2O_3 5 wt.%		
	S3 (300 °C)	S5 (600 °C)	S7 (900 °C)	S4 (300 °C)	S6 (600 °C)	S8 (900 °C)
ACI	0.543	1.332	1.073	0.658	1.114	1.053
H_{int} [Bqkg^{-1}]	0.647	1.559	1.223	0.728	1.211	1.159
D_{fw} [nGyh^{-1}], floor and walls	/	241.34/191.34*	193.07	/	197.24	187.36
D_{of} [nGyh^{-1}], only floor	/	86.20	68.94	/	70.44	66.90
D_{sup} [nGyh^{-1}], superficial material for all walls	/	42.8	34.22	/	34.96	33.20
$E_{indoor,fw}$ (mSv per year)	/	1.18/0.94*	0.95	/	0.97	0.92
$E_{indoor,f}$ (mSv per year)	/	0.42	0.34	/	0.35	0.33
$E_{indoor,sup}$ (mSv per year)	/	0.21	0.17	/	0.17	0.16

* This is not the excess exposure from building materials because concrete structures shield against gamma radiation from the undisturbed earth's crust. Using the average value of 50 nGyh^{-1} for the background, the excess dose rate in the room is therefore (241.34-50) nGyh^{-1} = 191.34 nGyh^{-1}

all walls. Due to, the annual effective dose of radiation of external exposure from all the investigated, thermally treated samples, does not exceed 1 mSv per year, if they are used like superficial material, these materials are acceptable for radiological aspect for the use as external insulation materials.

CONCLUSIONS

A detailed structural, physicochemical and radiological analysis of AAM doped with 1 wt.% and 5 wt.% Sm_2O_3 was performed in this research. The tested material showed great potential for application in everyday life in various branches of industry. It is very important to point out that from relatively low-cost raw materials we can get a useful and usable material for wide applications in industry – mechanical properties, corrosion resistance, and high durability in high-temperature applications. The XRF analysis confirmed the chemical composition (converted to oxides) dominated by silicon (IV)-oxide (SiO_2), aluminum (III)-oxide (Al_2O_3), and iron (III)-oxide (Fe_2O_3), which leads to excellent pozzolanic properties material. At elevated temperatures, the examined AAM proved to be very stable and the stoichiometric content of the oxide was slightly changed, while the pozzolanic activity was more pronounced in the sample with 1 wt.% Sm_2O_3.

The DRIFT method confirmed that thermal treatment changes the chemical bonds in AAM. The most significant changes occur at the highest temperatures. In this study, the largest change was observed in sample S7 treated at 900 °C, where the formation of the Sm-OH bond is most clearly seen. The XPS analysis showed that the investigated AAM has a very low (almost non-existent) carbon content, classifying this material as green-sustainable material for future applications. Based on the shift of the fitted O1s spectral lines, it can be concluded that with increasing temperature of thermal treatment, the amount of Si-OH and Si-ONa bonds increases, because with increasing temperature (maximum 900 °C) these bonds are regenerated and reconstructed. The SEM characterization additionally confirmed the structure and micro characteristics of the tested samples. It was clearly observed that the porosity and crystallinity of the grains increases with the increase in temperature. At 900 °C, the examined AAM were almost sintered. Better characteristics were observed in AAM doped with 5 wt.% Sm_2O_3, while a slightly less stable structure was noted in samples with 1 wt.% Sm_2O_3. It is obvious that the amount of Sm_2O_3 affects the stability of alkali- activated materials, by increasing the crystallinity and decreasing the pore size. Gamma spectrometric analysis showed that all the measured samples contain radionuclides (^{210}Pb, ^{226}Ra, ^{238}U, ^{235}U, ^{228}Ac (^{232}Th), ^{40}K) at concentrations within

typical ranges, whereby the presence of ^{137}Cs was not detected. Although the ACI for some tested materials is greater than 1, this does not pose a problem for commercial use and is considered safe for a surface construction material, because the *E* for that use, calculated according to the recommendations of the European Commission, does not exceed 1 mSv per year.

AUTHORS′ CONTRIBUTIONS

S. V. Knežević: writing – original draft, investigation, conceptualization. M. M. Ivanović: writing – review and editing, methodology, conceptualization, supervision. S. S. Nenadović: writing: review and editing, methodology, conceptualization. M. M. Rajačić: writing – review and editing, investigation, formal analysis. M. Nečemer: writing – review and editing, investigation, formal analysis. J. Potočnik: writing – review and editing, investigation, formal analysis, M. T. Nenadović: writing – review and editing, methodology, conceptualization.

ACKNOWLEDGMENT

This research was financially supported by the Ministry of Science, Technological Development and Innovation of the Republic of Serbia (contract No. 451-03-66/2024-03/200017).

The research was conducted under program grant No. 0402405, grant No. 1702402, and grant No. 1002404, the Vinča Institute of Nuclear Sciences, the National Institute of the Republic of Serbia, University of Belgrade, Serbia.

ORCID NO

S. V. Knežević: 0000-0002-9371-4066
M. M. Ivanović: 0000-0002-1152-4171
S. S. Nenadović: 0000-0003-4846-8801
M. M. Rajačić: 0000-0001-7004-4998
J. Potočnik: 0000-0001-7206-5952
M. T. Nenadović: 0000-0003-0503-2848

REFERENCES

[1] Kljajević, Lj., *et al*., S. Heat Treatment of Geopolymer Samples Obtained by Varying Concentration of Sodium Hydroxide as Constituent of Alkali Activator, *Gels, 8* (2022), 6, 333
[2] Song, H., *et Al*., Heavy Metal Fixing and heat resistance abilities of Coal Fly Ash-Waste Glass Based Geopolymers by Hydrothermal Hot Pressing, *Advanced Powder Technology, 29* (2018), 6, pp. 1487-1492
[3] Bakharev, T., Thermal Behaviour of Geopolymers Prepared Using Class F Fly Ash and Elevated Temperature Curing, *Cement and Concrete Research, 36* (2006), 6, pp. 1134-1147
[4] Siyal, A. A., *et al*., A Review on Geopolymers as Emerging Materials for the Adsorption of Heavy Metals and Dyes, *Journal of Environmental Management,* (2018), 224, pp. 327-339
[5] Fernandez-Jimenez, A., *et al*., Fixing Arsenic in Alkali-Activated Cementitious Matrice, *Journal of the American Ceramic Society, 88* (2005), 5, pp. 1122-1126
[6] Singh, N. B., *et al*., Geopolymers as an Alternative to Portland Cement: An Overview, *Construction and Building Materials, 237* (2020), 117455 https://doi.org/10.1016/j.conbuildmat.2019.117455
[7] Mladenović, N., *et al*., The Applications of New Inorganic Polymer for Adsorption Cadmium from Waste Water, *Journal of Inorganic and Organometallic Polymers and Materials,* (2020), 30, pp. 554-563
[8] Yu, L., *et al*., The Utilization of Alkali-Activated Lead-Zinc Smelting Slag for Chromite Ore Processing Residue Solidification/Stabilization, *International Journal of Environmental Research and Public Health, 18* (2021), 19, 9960 https://doi.org/10.3390/ijerph18199960
[9] Narasimharao, K., *et al*., Influence of Synthesis Conditions on Physico-Chemical and Photocatalytic Properties of Rare Earth (Ho, Nd, and Sm) Oxides, *Journal of Materials Research and Technology, 9* (2020), 2, pp. 1819-1830
[10] Ivanović, M., *et al.*, The Influence of Thermodynamic Parameters on Alkaline Activator of Geopolymers and Structure of Geopolymers, *Macedonian Journal of Chemistry and Chemical Engineering, 40* (2021), 1, pp. 107-117
[11] Nenadović, S. S., *et al.*, Structure Analysis of Geopolymers Synthesized from Clay Originated from Serbia, *Environmental Earth Sciences,* (2017), 76, pp. 1-10
[12] Kljajević, L. M., *et al*., Structural and Chemical Properties of Thermally Treated Geopolymer Samples, *Ceramics International, 43* (2017), 9, pp. 6700-6708
[13] Ivanović, M., *et al*., The Effect of the Concentration of Alkaline Activator and Aging Time on the Structure of Metakaolin Based Geopolymer, *Science of sintering, 52* (2020), 2, pp. 219-229
[14] Provis, J. L., Geopolymers and Other Alkali Activated Materials: Why, How, and What? *Materials and structures,* (2014), 47, pp. 11-25
[15] Zhang, H., *Building Materials in Civil Engineering*, Elsevier, 2011, Amsterdam, The Netherland
[16] Ivanović, M. M., *et al*., Physicochemical and Radiological Characterization of Kaolin and its Polymerization Products, *Materiales de Construccion, 68* (2018), 330 http://dx.doi.org/10.3989/mc.2018.00517
[17] ***, United Nations Scientific Committee on the Effects of Atomic Radiation. Sources and Effects of Ionizing Radiation, United Nations Scientific Committee on the Effects of Atomic Radiation (UNSCEAR) 2000 Report, Volume I: Report to the General Assembly, with Scientific Annexes-Sources, United Nations, https://doi.org/10.18356/49c437f9-en
[18] Nenadović, S. S., *et al.*, Chemical, Physical and Radiological Evaluation of Raw Materials and Geopolymers for Building Applications, *Journal of Radioanalytical and Nuclear Chemistry, 325* (2020), 2, pp. 435-445
[19] Nuccetelli, C., *et al*., Thorium Series Radionuclides in the Environment: Measurement, Dose Assessment and Regulation, *Applied Radiation and Isotopes, 66* (2008), 11, pp. 1657-1660
[20] Tsabaris, C., *et al*., Radioactivity Levels of Recent Sediments in the Butrint Lagoon and the Adjacent Coast of Albania, *Applied Radiation and Isotopes, 65* (2007), 4, pp. 445-453
[21] Beretka, J., *et al*., Natural Radioactivity of Australian Building Materials, Industrial Wastes and By-Products, *Health Physics, 48* (1985), 1, pp. 87-95
[22] Vukanac, I. S., *et al*., Assessment of Natural Radioactivity Levels and Radon Exhalation Rate Potential

from Various Building Materials, *Nucl Technol Radiat, 35* (2020), 1, pp. 64-73
[23] ***, WHO Handbook on Indoor Radon: a Public Health Perspective, World Health Organization, 2009, ISBN 978-92- 4- 154767- 3
[24] Cousins, C., *et al*., International Commission on Radiological Protection, *ICRP Publication,* (2011), 120, pp. 1-125
[25] Ramli, A. T., *et al*., Environmental ^{238}U and ^{232}Th concentration Measurements in an Area of High Level Natural Background Radiation at Palong, Johor, Malaysia, *Journal of Environmental Radioactivity, 80* (2005), 3, pp. 287-304
[26] Nenadović, S., *et al*., Vertical Distribution of Natural Radionuclides in Soil: Assessment of External Exposure of Population in Cultivated and Undisturbed Areas, *Science of the Total Environment, 429* (2012), 2, pp. 309-316
[27] Lilek, N., *et al*., Use of EDXRF Elemental Fingerprinting for Discrimination of Botanical and Geographical Origin of Slovenian Bee Pollen, *X-Ray Spectrometry, 51* (2022), 3, pp. 186-197
[28] Nečemer, M., *et al*., Application of X-Ray Fluorescence Analytical Techniques in Phytoremediation and Plant Biology Studies, *Spectrochimica Acta Part B: Atomic Spectroscopy, 63* (2008), 11, pp. 1240-1247
[29] Stojanović, Z. S., *et al*., *Measurement of Particle Size Distribution by Laser Light Diffraction Methody* (in Serbian), Tehnika-Novi Materijali, 2010, 1-15
[30] Guidebook, A., *Measurement of Radionuclides in Food and the Environment*, Vienna: International Atomic Energy Agency, 1989
[31] Kaya, Y., *et al*., Investigation of Pozzolanic Activity of Recycled Concrete Powder: Effect of Cement Fineness, Grain Size Distribution and Water/Cement Ratio., Materials Today: *Proceedings*, (2023)
[32] The ASTM, C., Standard Specification for Concrete Aggregates, American Society for Testing and Materials, Philadelphia, Penn., USA, 2003
[33] Bahram, K., *et al*., Synthesis and Characterization of Nd_2O_3 Nanoparticles Using Urea as Precipitation Agent, *Journal of Transition Metal Complexes*, (2023), 10.32371/jtmc/246148
[34] Beuls, A., *et al*., P. Methanation of CO_2: Further Insight Into the Mechanism Over $Rh/\gamma\text{-}Al_2O_3$ Catalyst, *Applied Catalysis B: Environmental*, (2012), 113, pp. 2-10
[35] Nenadović, S. S., *et al*., Structural and Chemical Properties of Geopolymer Gels Incorporated with Neodymium and Samarium, *Gels, 7* (2021), 4, p. 195
[36] Kljajević, L. M., *et al.*, Structural and Chemical Properties of Thermally Treated Geopolymer Samples, *Ceramics International, 43* (2017), 9, pp. 6700-6708
[37] ***, European Commission (EC), Radiation protection 112-Radiological Protection Principles concerning the Natural Radioactivity of Building Materials. Directorate-General Environment, Nuclear Safety and Civil Protection, 1999
[38] Markkanen, M., Radiation Dose Assessments for Materials with Elevated Natural Radioactivity, Report STUK-B-STO 32, Radiation and Nuclear Safety Authority- STUK, 1995

Received on January 16, 2025
Accepted on March 10, 2025

Сања В. КНЕЖЕВИЋ, Марија М. ИВАНОВИЋ, Снежана С. НЕНАДОВИЋ, Милица М. РАЈАЧИЋ, Маријан НЕЧЕМЕР, Јелена ПОТОЧНИК, Милош Т. НЕНАДОВИЋ

РАДИОЛОШКА КАРАКТЕРИЗАЦИЈА АЛКАЛНО АКТИВИРАНОГ МАТЕРИЈАЛА ДОПИРАНОГ СА SM_2O_3 И ЊЕГОВИХ ПРОИЗВОДА ПОЛИМЕРИЗАЦИЈЕ

Циљ овог рада био је одређивање радиолошке карактеризације алкално активираног материјала са Sm_2O_3 и његовим продуктима полимеризације. Синтетисани су алкално активирани материјали са додатком 1 мас.% и 5 мас.% Sm_2O_3 и одређена је природна радиоактивност. Енергетска дисперзивна рендгенска флуоресценција показала је промене у фазном саставу или формирање стабилних једињења на вишим температурама. Сви узорци показују добру пуцоланску активност, док је проценат Sm_2O_3 незнатно промењен. Рендген фотоелектронска спектроскопија потврдила је да добијени материјал има веома низак садржај угљеника и да је као такав потпуно еколошки због ниског угљеничног отиска. Детаљна анализа пика кисеоника указује на варијације у стехиометрији оксида, које могу утицати на промену вредности природне радиоактивности. Скенирајућа електронска микроскопија потврдила је да повећањем температуре термичке обраде долази до отварања пора у алкално активираном материјалу, као и даљег ширења реакције повећања порозности и кристализације. Радиолошким мерењем је потврђено да је испитивани алкално активирани материјал безбедан за употребу и експлоатацију. Треба нагласити да присуство вештачког радионуклида цезијум ^{137}Cs није детектовано.

Кључне речи: алкално активирани материјал, Sm_2O_3, гама спектрометрија, енергетска дисперзивна рендгенска флуоресценција, рендген фотоелектронска спектроскопија